공학석사학위논문

Optimal thickness ratio of the bilayer anode for performance enhancement in thin film solid oxide fuel cells

박막 고체산화물 연료전지의 성능향상을 위한 이중층 연료극의 최적의 두께비에 대한 연구

2015년 8월

서울대학교 대학원

기계항공공학부

노 승 탁

Optimal thickness ratio of the bilayer anode for performance enhancement in thin film solid oxide fuel cells

박막 고체산화물 연료전지의 성능향상을 위한 이중층 연료극의 최적의 두께비에 대한 연구

지도교수 차 석 원

이 논문을 공학석사 학위논문으로 제출함

2015년 5월

서울대학교 대학원
기계항공공학부
노 승 탁

노승탁의 공학석사 학위논문을 인준함

2015년 5월

위 원 장 주 종 남 (인)

부위원장 차 석 원 (인)

위 원 안 성 훈 (인)

Abstract

Optimal thickness ratio of the bilayer anode for performance enhancement in thin film solid oxide fuel cells

Seungtak Noh

School of Mechanical and Aerospace Engineering

The Graduate School

Seoul National University

Mixed ionic-electronic conductors (MIECs) attracts increased attention for several advantages, such as expanded triple phase boundaries (TPBs) or replacement of platinum-based catalysts. In the present study, performance of thin film SOFCs comprised of nickel oxide-gadolinia doped ceria (NiO-GDC) anode, yttria stabilized zirconia (YSZ) electrolyte and Pt cathode was analyzed using potentiodynamic technique. The whole components of the cells were fabricated by reactive sputtering technique, and then sputtering time in the anode deposition process was especially varied from 6h to 10h with 2 hours intervals to investigate effect of anode thickness on the cell performance. Electrochemical performance of the cells was evaluated in an electric furnace of 500^{o}C, with 100 standard cubic centimeter per minute (sccm) hydrogen gas at anode side. The cell with 320 nm-thick NiO-GDC layer exhibited the best performance (105 mW/cm^{2}). Electrochemical impedance spectroscopy (EIS)

revealed ohmic resistance of the cells were affected by anode thickness. The electrical conductivity of NiO-GDC is significantly smaller than that of pure nickel at low temperatures. Thus, relatively high ohmic resistance of NiO-GDC anode remains a significant problem.

We additionally deposit Ni layer to overcome high ohmic resistance of the NiO-GDC anode. A 70 nm-thick Ni layer deposited between the NiO-GDC anode and the anodic aluminum oxide (AAO) substrate successfully enhanced the electrochemical performance of thin film solid oxide fuel cells (TF-SOFCs) using the sputtering technique. The thickness ratio between the NiO-GDC and Ni layer on the cell performance was investigated. The TF-SOFCs with sputtered 210 nm-thick NiO-GDC and 70 nm-thick Ni layers exhibited maximum power density of 170 mW/cm^2 at 500 ^oC, which was about two times higher than those without Ni layers (80 mW/cm^2). The EIS data showed that the performance improvement mostly stems from two factors: the reduced ohmic and anodic activation resistances and the improved anodic kinetics. When the NiO-GDC layer is too thin (70 nm), the ionic conduction in the NiO-GDC layer became sluggish. Therefore, the maximum power density decreased to 132 mW/cm^2. Thus, we can conclude a proper thickness ratio between the NiO-GDC and Ni layers is required to maximize cell performance.

Keywords : Nickel, nickel oxide-gadolinia-doped ceria, nickel, thin film-solid oxide fuel cells, bilayer anode, sputter

Student Number : 2013-23066

Contents

List of Tables

List of Figures

1. Introduction

1.1. Background of the study

A fuel cell is a device that directly converts the chemical energy of fuel into electrical energy by a chemical reaction [1]. All types of fuel cells consist of two electrodes called the anode and the cathode, and one electrolyte, and generate electricity by fuel oxidation reaction at the anode and oxygen reduction reaction at the cathode. Unlike conventional combustion engines, direct energy conversion by chemical reaction enables highly efficient operation, and are free to *Carnot* cycle efficiency. Also fuel cells have size-independent property unlike batteries, e.g. maximizing capacity only by increasing fuel reservoir size. A product of the electrochemical reaction is just H_2O, therefore most fuel cells are largely exempt from environmental issues. The multiple advantages make a fuel cell a promising clean energy and attractive candidate as an alternative energy source.

There are several types of the fuel cells, and it depends on what kind of the electrolyte is employed for. Generally, it could be classified polymer membrane fuel cells (PEMFCs), solid oxide fuel cells (SOFCs), molten carbonate fuel cells (MCFCs), phosphoric acid fuel cells (PAFCs) and alkaline fuel cells (AFCs). The main difference of the fuel cells is operating temperature which is mainly decided by the electrolyte material. In case of PEMFCs, the operating temperature is confined to 80 ^{o}C due to the property of polymer electrolyte. Detailed information about operating temperature for the several kinds of fuel cells is followed in table 1.1.

Table 1.1 Fuel cell types

	PEMFCs	**PAFCs**	**AFCs**	**MCFCs**	**SOFCs**
Electrolyte	Polymer membrane	Liquid H_3PO_4	Liquid KOH	Molten carbonate	Ceramic
Charge Carrier	H^+	H^+	OH^-	CO_3^{2-}	O_2^-
Operating temperature	80 ^oC	200 ^oC	60-220 ^oC	650 ^oC	600 – 1000 ^oC
Catalyst	Platinum	Platinum	Platinum	Nickel	Perovskites
Fuel compatibility	H_2, methanol	H_2	H_2	H_2,CH_4	H_2, CH_4, CO

1.2 Solid oxide fuel cells

SOFCs, which employ solid ceramic materials as electrolytes, have received considerable attention. Compared to other fuel cells, SOFCs have several advantages such as use of non-precious catalyst, flexibility in the choice of fuel including hydrocarbon fuels, low cost and relatively high-efficiency [1]. The high operating temperature of SOFCs (i.e. 800-1000 ^{o}C), however, has many drawbacks like fast thermal degradation, expensive thermal resistance materials, sealing issues, and long start-up times [1]. At high temperature, for example, electrode materials are easily agglomerated, and cell interconnect issues and sealing problem begin to emerge.

Various research has been conducted to reduce the operating temperature of the thin film SOFCs (TF-SOFCs) [2-7]. TF-SOFCs are leading candidate to overcome high ohmic resistance of electrolyte at a low temperature. Typically, the electrolyte of the TF-SOFCs has a thickness less than 1μm, therefore ohmic loss originated from sluggish ionic transport in the electrolyte can be compensated. Therefore, the ohmic resistance decreases due to the reduction in electrolyte thickness.

There are several technologies that contribute to development of the TF-SOFCs. By a vacuum deposition technique (e.g. physical vapor deposition (PVD) and chemical vapor deposition (CVD)), a thin electrolyte layer and an electrode layer can be fabricated. Also, nano-scale particles fabricated by the vacuum deposition technique increase the electrochemically active specific area to reduce the activation resistance of the cell. The obtained films normally have fine micro-structure

compared to conventional bulk cell, which maximize triple phase boundaries (TPBs) area at the electrode-electrolyte interface. Therefore, the performance drop at low operating temperatures can be compensated [8-9].

Another way to reduce the operating temperature is to choose electrochemically active materials even at low electrode temperatures. For fuel cells, an electrochemical reaction can only take place at TPBs where electrolyte, electrode, and gas are in contact. An increase in reaction rate can be achieved by maximizing the triple phase boundary (TPB) density [1]. The employment of mixed ionic electronic conductor (MIECs) electrodes such as nickel oxide/yttria-stabilized zirconia (NiO-YSZ), nickel oxide/gadolinia-doped ceria (NiO-GDC), and nickel oxide/samaria-doped ceria (NiO-SDC) for the anode in addition to lanthanum strontium cobalt ferrite (LSCF) and lanthanum strontium manganite (LSM) for the cathode may be a solution, because TPB density can be increased from the electrolyte/electrode interface (2D) to the entire electrode region (3D). As a result, activation loss can be significantly reduced by using MIECs [10-13].

1.3 NiO-GDC

Among the MIEC anode materials mentioned previously, NiO-YSZ matches well with YSZ electrolyte's thermal expansion and has chemical stability over a wide temperature range [14]. Nevertheless, the ionic conduction in YSZ composite is sluggish at low temperatures (400-600 ^{o}C) and the ohmic resistance significantly increases. On the other hand, GDC has higher ionic conductivity than YSZ, [1, 10] which may make GDC more suitable for the application of low temperature SOFCs.

Compared to pure nickel, NiO-GDC has been believed to enlarge TPB density and lower faradaic resistance [15]. The electrical conductivity of NiO-GDC, however, is significantly smaller than that of pure nickel at low temperatures. Thus, the resultant high ohmic resistance of the NiO-GDC electrode could be problematic[12, 15-16].

1.4 Objectives and scopes

1.4.1 NiO-GDC anode

In this study, we employed NiO-GDC as an anode of the low temperature TF-SOFCs. Compared to NiO-YSZ which is typically used for an anode of a high temperature SOFCs, NiO-GDC has a superior ionic conductivity at a low operating temperature and electric conductivity a low oxygen condition. These properties makes NiO-GDC suitable for an anode of a low temperature SOFCs.

Several studies about a NiO-GDC anode have been conducted, effects of anode thickness variation on the cell performance is unrevealed. By controlling sputtering time, we modulated thickness of the anode layer. Thickness of the anode layer is expected to affect triple phase boundaries (TPBs) length. Because thicker MIECs anode enlarges TPBs length, and hydrogen oxidation reaction (HOR) can be easily activated. Thicker anode, however, makes ion transport path longer, and ohmic resistance is increased.

We used nano-porous anodic aluminum oxide (AAO) as a substrate, and surface morphology is another factor to determine the cell performance. There exists a correlation between thickness of the anode and surface morphology.

TF-SOFCs comprised of Pt cathode, YSZ electrolyte and NiO-GDC anode were fabricated. Three kinds of TF-SOFCs with different anode thickness were fabricated, and a cell test was conducted at a low operating temperature of a 500 ^{o}C. To investigate resistances which affect the cell performance, the electrochemical

impedance spectroscopy (EIS) data was collected.

1.4.2 NiO-GDC | Ni bilayer anode

To overcome high ohmic resistance of NiO-GDC anode, the TF-SOFCs comprised of (cathode)Pt | YSZ | NiO-GDC | Ni(anode) were fabricated. In order to improve the electrical conductivity of the NiO-GDC anode, we deposited Ni current collection layer between the NiO-GDC film and nanoporous AAO substrate [17]. Several TF-SOFCs with different Ni to NiO-GDC bilayer anode thickness ratio were fabricated and analyzed for the cell performance of both Ni and NiO-GDC layers thickness. As mentioned above, ohmic loss in the bilayer anode was influenced by the additional Ni layer thickness. The NiO-GDC layer thickness also affected the ohmic resistance size. Electrochemical characterizations such as open circuit voltage measurement, current-voltage characterization, and electrochemical impedance spectroscopy (EIS) were evaluated at 500 ^{o}C.

2. Experimental

2.1 Preparation of the cell

2.1.1 NiO-GDC anode

We fabricated three TF-SOFCs comprised of Pt (cathode) | YSZ (electrolyte) | NiO-GDC (anode) on a nano-porous ceramic AAO template (Synkera Technology Inc., U.S.A.). The schematic of the cell is presented in figure 2.1. The free-standing AAO template in 1x1cm^2 size had thickness of 100 μm and uniformly distributed 80 nm-diameter pores. A dense NiO-GDC anode was deposited on the AAO template by sputtering technique. A RF sputtering power of 50 W was applied to commercial NiO-GDC target (50:50 weight percent, NiO-(CeO2)0.9 (GdO1.5)0.1, RnD Korea, Korea) with a mixed Ar/O_2 gas of 0.93 Pa. The anode thickness gradually changed from 240 nm to 400 nm by adjusting sputtering time.

In all TF-SOFCs, the electrolyte thickness and the cathode thickness were maintained constant at 750 nm and 200 nm, respectively. 750 nm-thick YSZ layer was deposited from Zr-Y alloy target (16 atomic percent Y, 84 atomic percent Zr, Advantec Korea, Korea) with RF power of 200 W at a mixed Ar/O2 gas (O2/Ar ratio : 20 %). Lastly, a porous Pt cathode was deposited on the electrolyte layer under the Ar pressure of 12 Pa at a DC gun power of 100 W. The effective area of the

cathode was defined to be 0.1 x 0.1 cm^2 by a shadow mask. The target to the substrate distance was set at 8 cm, and all sputtering processes were conducted at a room temperature.

2.1.2 NiO-GDC| Ni bilayer anode

We utilized commercial AAO template (Synkera Technology Inc., U.S.A.) with 80 nm pore diameter and 100 μm thick substrates of the TF-SOFCs. As shown in figure 2.2, Ni, NiO-GDC, YSZ, and Pt layers were sequentially deposited on a 1 x 1 cm^2 AAO membrane substrate. The TF-SOFCs with anodes of different Ni/NiO-GDC thickness ratios and same total thickness were prepared to investigate the effect of the Ni layer on the cell performance. Detailed information is provided in table 2.1. We named the three TF-SOFCs as cell 4, cell 5, and cell 6, respectively.

A thin Ni layer was deposited on the AAO substrate using a metal Ni target (99.99 %, RnD Korea, Korea) by direct current (DC) magnetron sputtering at an Ar pressure of 4Pa. (99.999 %) with sputtering power set to 100 W. Subsequently, a dense NiO-GDC layer was deposited on the Ni layer using commercial NiO-GDC targets (50:50 weight percent, NiO-$(CeO_2)_{0.9}$ $(GdO_{1.5})_{0.1}$, RnD Korea, Korea) by radio frequency (RF) magnetron sputtering at a mixed Ar/O_2 gas (O_2/Ar ratio: 20 %) at 0.93 Pa and sputtering power set to 50 W. The Ni to NiO-GDC thickness ratios were controlled by the sputtering time. Detailed information is presented in table 2.2.

A RF sputtering power of 200 W was applied to the Zr-Y alloy target (16 atomic

percent Y, 84 atomic percent Zr, Advantec Korea, Korea) with a mixed Ar/O_2 gas at 0.67 Pa. A fully dense YSZ electrolyte was successfully deposited on the top of the bilayer anode. Finally, a porous Pt cathode was sputtered by using DC plasma at 100 W under Ar pressure of 12 Pa. The effective area was controlled to 0.1 x 0.1 cm^2 using a physical shadow mask. For each sputtering process, the distance between the target and the substrate was maintained at 80 mm and the substrate temperature was set at room temperature.

Figure 2.1 Schematic of cell 1, cell 2 and cell 3

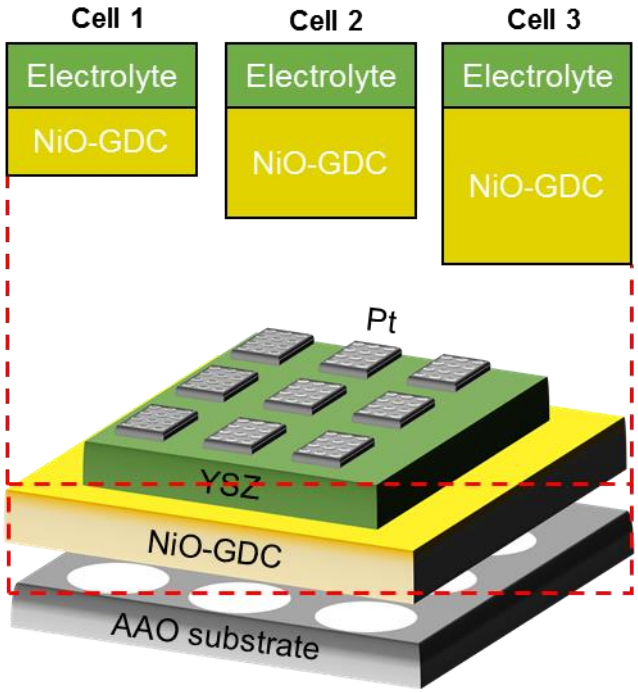

Figure 2.2 Schematic of cell 4, cell 5 and cell 6

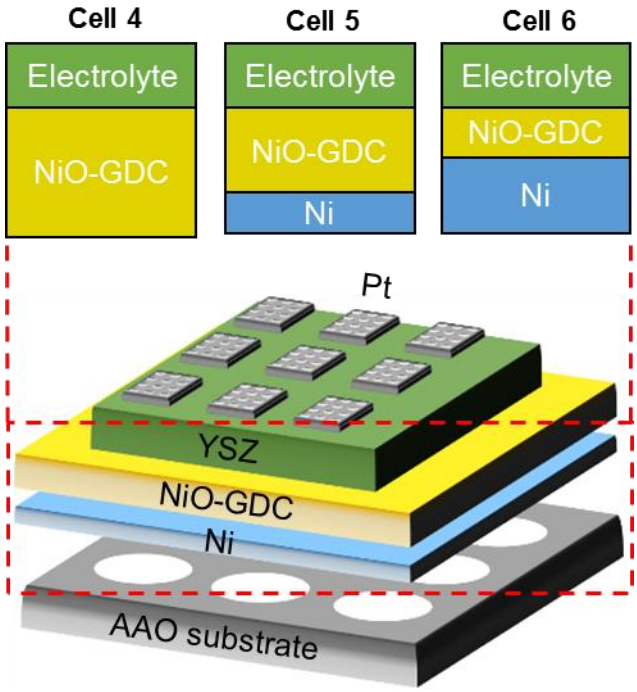

Table 2.1 Detailed information about cell 4, cell 5 and cell 6

	Thickness (nm)			
	Anode		Electrolyte	Cathode
	Ni	NiO-GDC	YSZ	Pt
Cell 4	0	280	600	150
Cell 5	70	210	600	150
Cell 6	210	70	600	150

Table 2.2 Detailed information about sputtering time of the bilayer anode (cell 4/5/6)

	Sputtering time	
	Ni	NiO-GDC
Cell 4	0	7h
Cell 5	2m 45s	4h 40m
Cell 6	8m 15s	1h

2.2 Electrochemical performance measurement

The electrochemical performance of the cells was measured with a custom-made test station in an electric furnace at 500 ^{o}C [18-21]. Dry hydrogen (99.999%) was supplied to the anode side with a flow rate of 100 sccm, and the cathode side was exposed to the ambient atmosphere. For the current collection, a hardened-steel probe (Leeno Inc., Korea) was directly contacted to the cathode while a 0.5 mm diameter silver wire was connected to the anode using silver paste (597A, Aremco products, U.S.A.).

Polarization curves and impedance spectra were obtained using an impedance analyzer (Solartron analytical 1260/1287, Solatron, U.K.). The polarization curves were acquired by using the potentiodynamic technique with a 30 mV/s scan rate. Electrochemical impedance spectroscopy (EIS) was conducted at OCV with the AC voltage at 30 mV amplitude in the 2 Hz to 1 MHz frequency range.

2.3 Electrochemical performance measurement

2.3.1 NiO-GDC anode

Surface and cross-sectional images of the TF-SOFCs was investigated by focused ion beam-scanning electron microscopy (FIB-SEM, Quanta 3D FEG, FEI company, U.S.A.) with the operating voltage of 5 kV. The only NiO-GDC sputtered sample was analyzed by energy dispersive x-ray spectroscopy (FESEM-EDS, S-4800,

Hitachi, Japan) for investigation of the anode surface. After cross-sectional images were obtained, thickness of the electrodes and electrolyte were measured.

2.3.2 NiO-GDC| Ni bilayer anode

To investigate the chemical composition ratio of the NiO-GDC layer, field emission scanning electron microscopy with energy dispersive x-ray spectroscopy (FESEM-EDS, S-4800, Hitachi, Japan) analysis was conducted. Cross-sectional structural images of TF-SOFCs were acquired to measure the thickness of each layer by using focused ion beam-scanning electron microscopy (FIB-SEM, Quanta 3D FEG, FEI company, U.S.A.) at the operating voltage of 5 kV.

3. Results and Discussion

3.1 NiO-GDC anode

Figure 3.1 (a)-(c) show cross-sectional images of the tested cells measured by FIB-FESEM. NiO-GDC anode layer, YSZ electrolyte layer and Pt cathode layer were sequentially sputter-deposited on AAO substrate. In middle layer, electrolyte, no pinholes and connected cracks are detected, and we can speculate that fuel crossover or short current through the electrolyte was not happened. All TF-SOFCs have 750 nm-thick electrolyte and 200 nm-thick cathode. The anode thickness of the cell 1-3 have 240 nm, 320 nm and 400 nm, respectively.

The figure 3.2 showed I-V curves of the TF-SOFCs obtained at 500 ^{o}C. The open circuit voltage (OCV) of cell 1, cell 2 and cell 3 were 1.14 V, 1.15 V and 1.11 V, respectively. These OCV values seem to be little different with the values in previous researches using similar cell fabrication method. Fuel crossover or short circuit current problems, therefore, was not happened because of dense and tight YSZ electrolyte structure [3, 19].

The maximum power density of cell 1, cell 2 and cell 3 were measured 49, 109 and 83 mW/cm^2, respectively. Compared to cell 1, cell 2 which have 80 nm thicker anode layer than cell 1 exhibited much higher electrochemical performance. The maximum power density was decreased to 83 mW/cm^2 as anode thickness was increased from 320 nm to 400 nm.

Figure 3.1 FIB-SEM cross-sectional images of (a) cell 1, (b) cell 2 and (c) cell 3

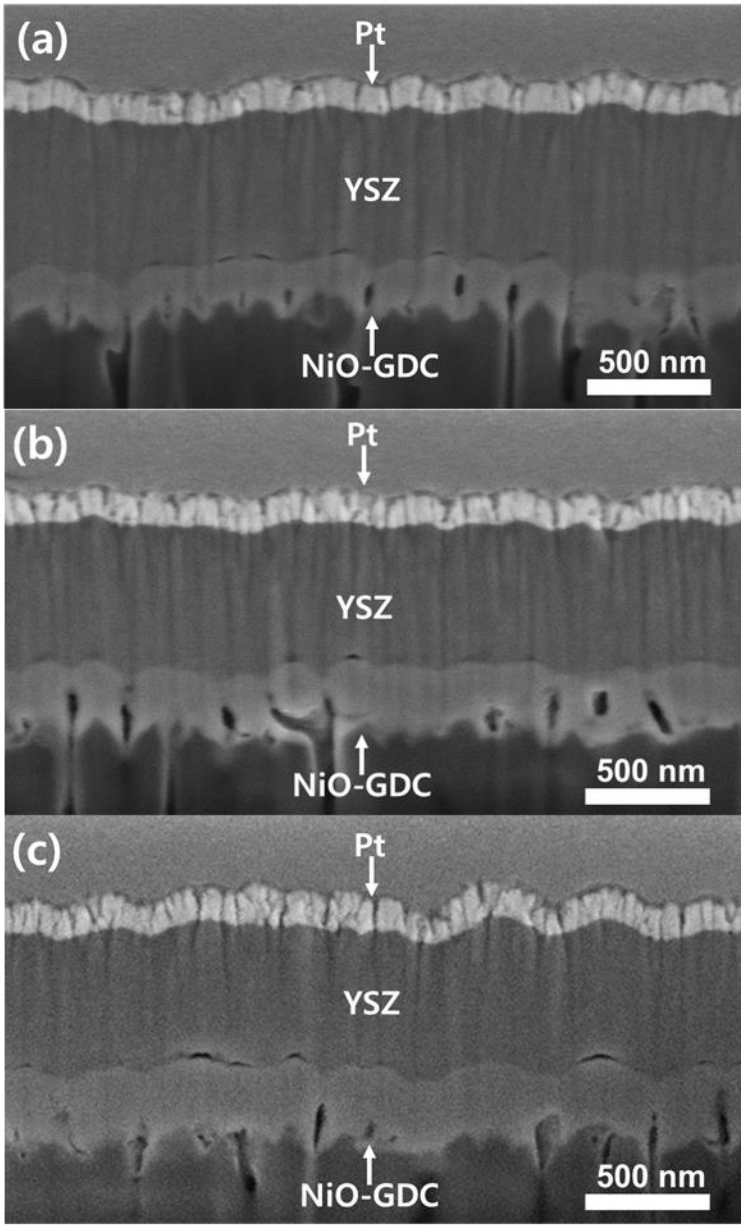

Figure 3.2 I-V curves of cell 1, cell 2 and cell 3

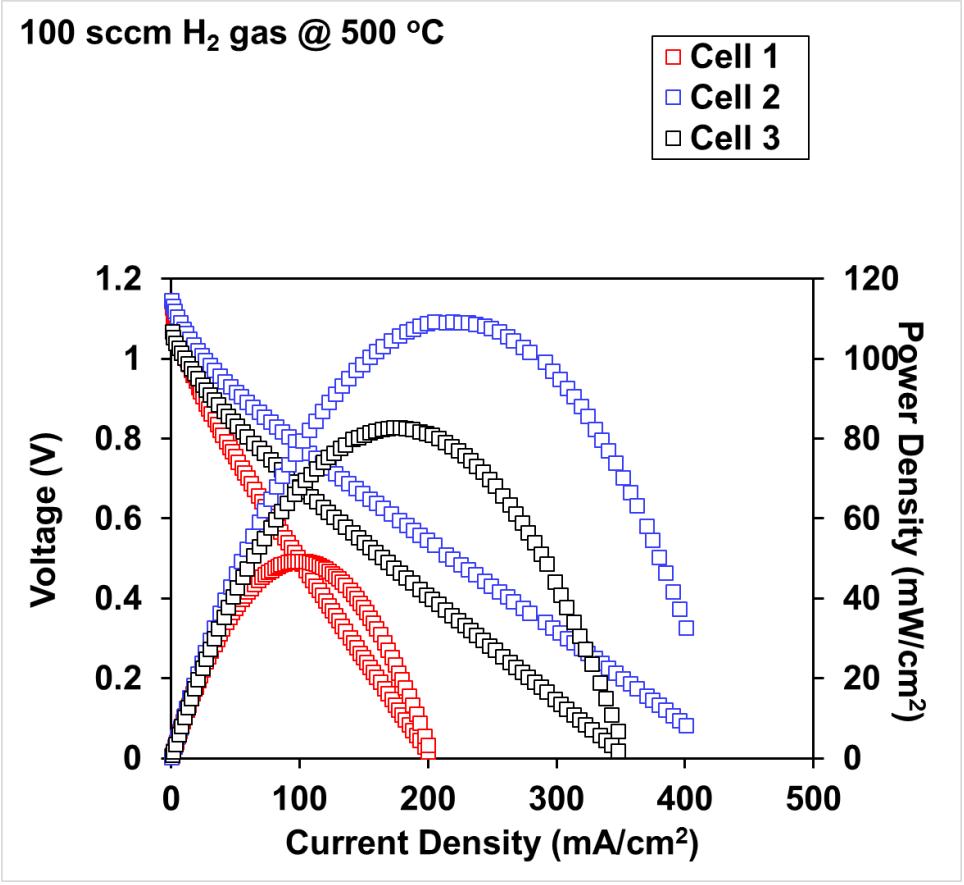

To compute the individual contributions such as ohmic resistance, faradaic resistance and mass transport resistance, EIS analysis was conducted. The nyquist plots of impedance spectra of the cells measured at 0.5 V bias were presented in figure 3.3(a). By fitting procedure to the equivalent circuit model shown in figure 3.3(b), the individual resistances were estimated, and denoted as R1 (Ohmic resistance), R2 (Electrolyte), R3(Anode activation), R4(Cathode activation) [3, 20].

R1, R2, R3 and R4 represented the high frequency (HF) intercept, the HF semi-circle, the intermediate frequency (IF) semi-circle and the low frequency (LF) semi-circle, respectively. Firstly, HF intercept was speculated as the sum of the electronic resistance and resistance from ionic transport process in MIECs anode. To investigate the HF semi-circle found in all plots, we analyzed the impedance spectra obtained at OCV and 0.5 V in figure 3.4. The size of HF semi-circle is independent on DC bias voltage. In previous research, the HF semi-circle that does not depend on bias voltage indicates ionic resistance of the electrolyte [5]. In this study, the HF semi-circles in all plots can be considered as ionic resistance of the YSZ electrolyte, and we denote R1+R2 as total ohmic resistance. The total ohmic resistance of cell, cell 2 and cell 3 were measured 3.45, 1.13 and 2.16 $\Omega \cdot cm^2$.

Figure 3.3 (a) Impedance spectra of cell 1, cell 2 and cell 3 at 500°C

(b) Equivalent circuit model

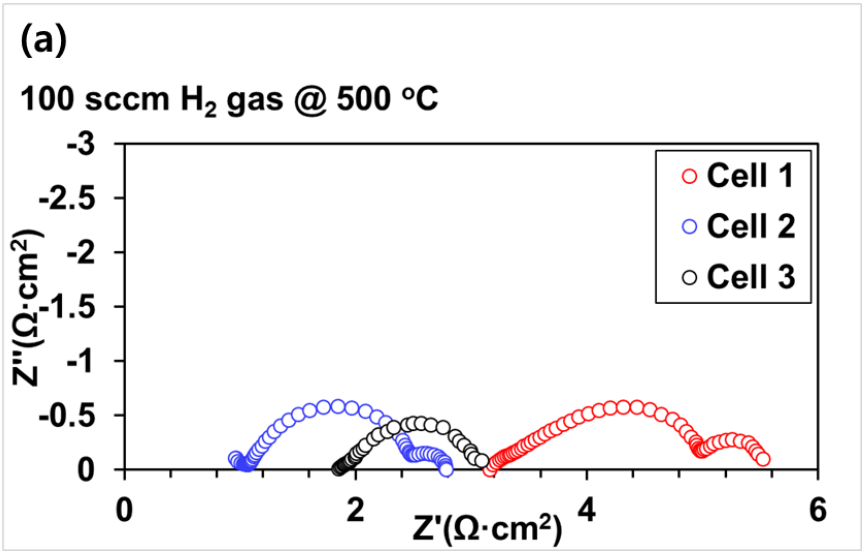

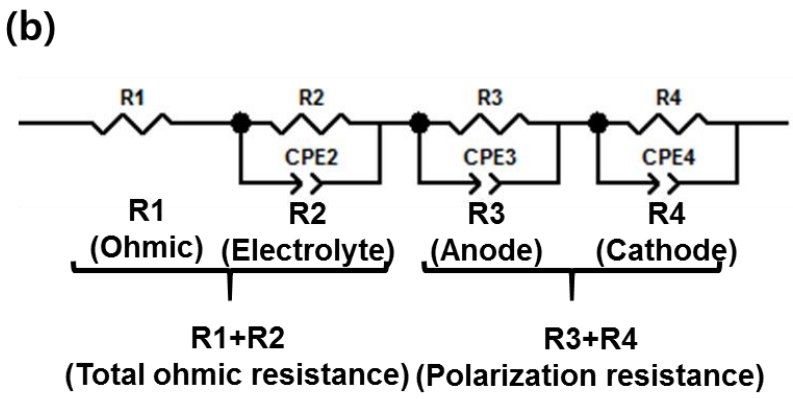

Figure 3.4 Nyquist plot of the impedance spectra under OCV and 0.5 V bias at 500ºC (a) cell 1 (b) cell 2 (c) cell 3

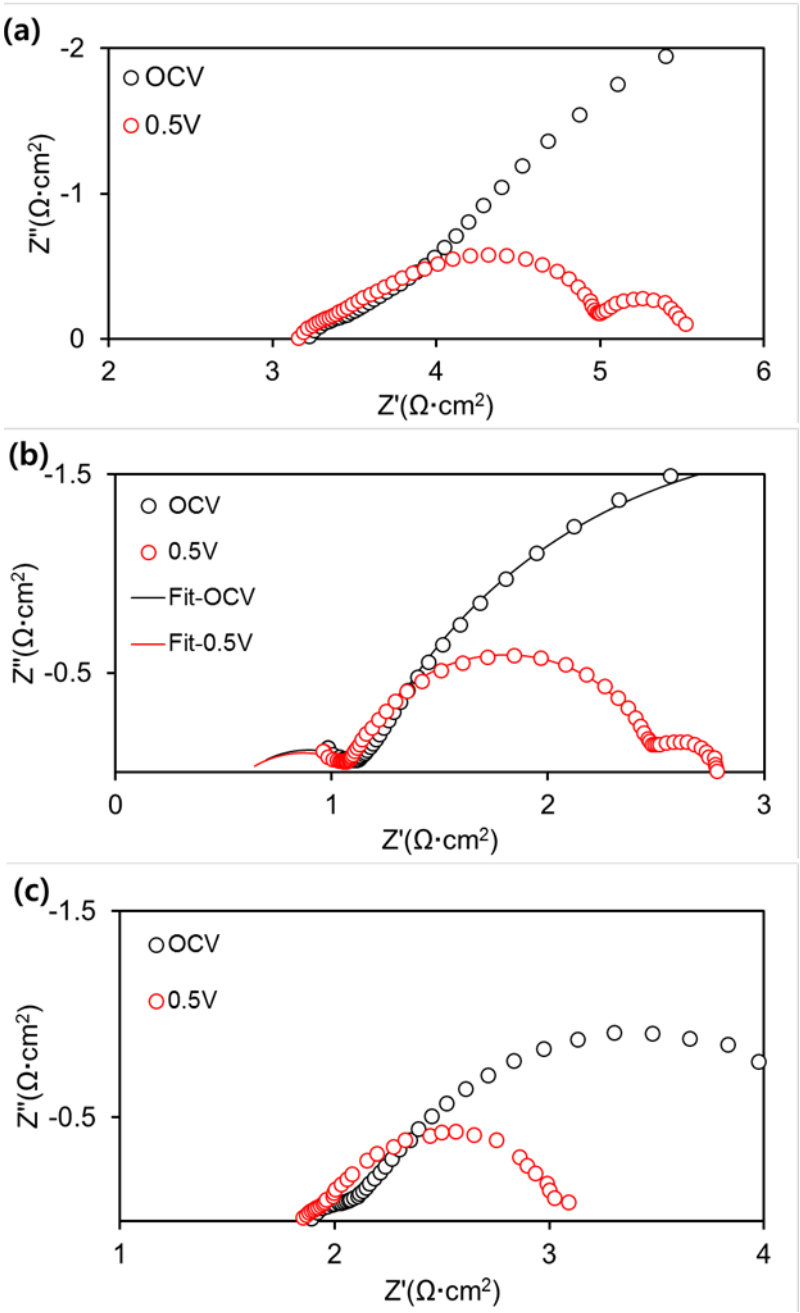

Considering that all cell components have identical composition except the anode, these ohmic resistance difference was originated from the anode. At the anode, there are two factors which contribute ohmic resistance, and they are shown in figure 3.5. Firstly, anode ionic resistance occurs when oxygen ion transmitted from electrolyte is vertically conducted in MIECs anode (factor 1). It is assumed that anode ionic resistance is directly proportional to the thickness, because thicker anode makes ion transfer path longer. Secondly, anode electronic resistance is another factor that contributes ohmic resistance (factor 2). Through hydrogen oxidation reaction (HOR), electrons are generated, and conducted to current collector (Ag paste) in parallel to the cell. In this case, anode electronic resistance is in inverse proportion to the thickness, because current collection in parallel direction would be hampered at extremely thin anode layer.

Considering extremely thin anode thickness (240 nm), it seems clear that anode electronic resistance (factor 2) has greater influence on the ohmic resistance at cell 1. At cell 3, however, thick MIECs anode extended ion transfer path, and anode ionic resistance was increased (factor 1). At cell 2 which has intermediate range thickness among three cells, ohmic resistance was measured minimum value (1.13 $\Omega \cdot cm^2$). This result indicates that the sum of electronic and ionic resistance was minimized, appropriate anode thickness, therefore, is highly required to reduce ohmic resistance.

Fig. 3.5 Schematic of current collection and oxygen ion transport mechanism at the anode. Electron transfer to Ag paste in parallel to the cell (solid line), and ion transfer in perpendicular to the cell (dotted line)

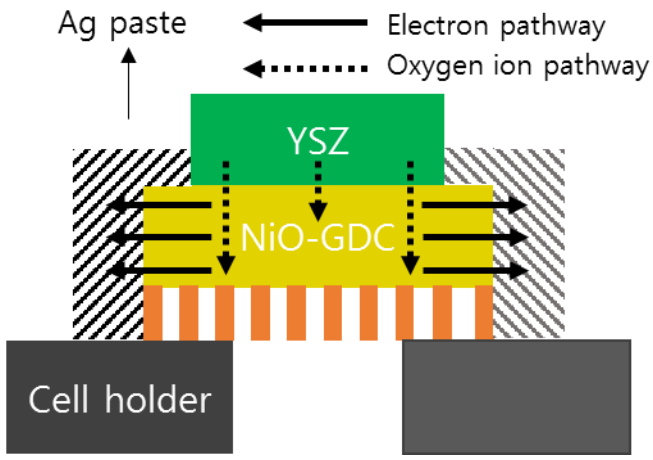

As previously mentioned, IF and LF semi-circles indicate anode faradaic resistance and cathode faradaic resistance, respectively [20]. Because LF semi-circle is independent on the anode thickness variation, LF semi-circles are obviously faradaic resistance originated from Pt cathode. Meanwhile, the size of the IF semi-circles seem to be changed along with thickness variation. As anode thickness was increased (Cell 1 < Cell 2 < Cell 3), semi-circle size was decreased. This correlation can be explained by the fact that increased anode thickness expands TPBs sites in the anode. At expanded TPBs sites, HOR can be effectively activated, and the anode faradaic resistance associated with activation loss was steadily decreased (1.57 $\Omega \cdot cm^2 \rightarrow$1.36 $\Omega \cdot cm^2 \rightarrow$0.86 $\Omega \cdot cm^2$).

Thickness difference also had a strong influence on surface morphology of the anode. Figure 3.6 show surface morphologies of the NiO-GDC anode layers deposited on AAO substrate. As anode thickness is increased [(a)→(b)→(c)], pore size becomes smaller, and the morphology seems to be denser. Also, relatively fine particles are observed. For this reason, reaction area at the anode/electrolyte interface can be enlarged. The reason that anode structure becomes denser and composed of finer particles at thicker anode is nano-porous substrate with 80 nm-diameter. When anode layer didn't have sufficient thickness (e.g. cell 1), sputtered particles were only deposited around lattice sites in substrate. In this case, TPBs region was confined to lattice frame. As anode thickness was increased, sputtered particles were stacked on the interstitial lattice, and expanded TPBs sites. This perspective also explains decrease in anode faradaic resistance at the thicker anode.

Figure 3.6 Surface images of NiO-GDC films. (a) cell 1 (b) cell 2 (c) cell 3

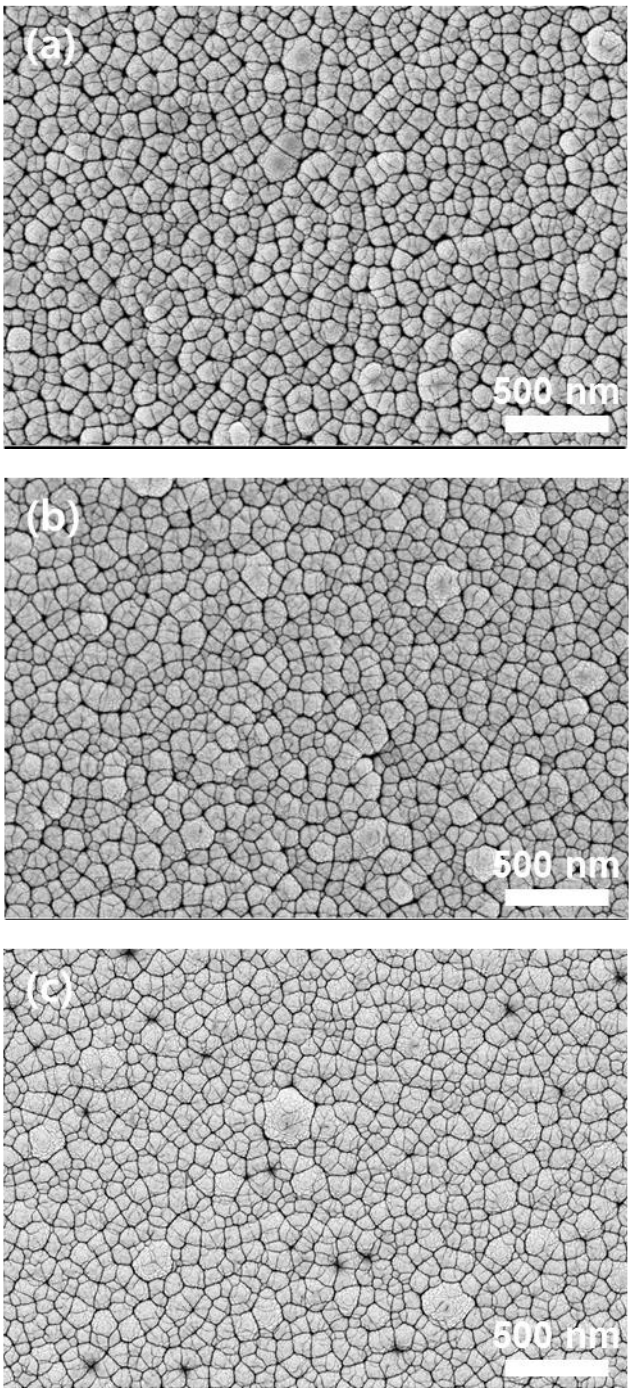

3.2 NiO-GDC| Ni bilayer anode

Figure 3.7 presents the surface morphology and chemical composition of the NiO-GDC film deposited on the AAO template. As shown in figure 3.7(a), the NiO-GDC film deposited on the AAO substrate shows fine-grained and nanoporous morphology. Figures 3.7(b)-(d) present the EDS composition mapping of Ni, Ce, and Gd elements at the surface shown in figure 3.7(a), visualized by different colors. As expected, Ni, Ce, and Gd atoms are uniformly distributed on the surface of NiO-GDC films, which implies TPB sites are also uniformly distributed over the entire NiO-GDC electrode. The chemical composition ratios of the NiO-GDC film are obtained. The measured atomic concentration of Ni on the film surface is 26.5 %, which is close to the values presented in previous reports and sufficient enough to facilitate hydrogen oxidation at the TPB [22-23]. The Ce concentration (22.4 %) to Gd content (2.54 %) ratio of the film is 8.80, which is similar to that of the target (9:1). This result indicates that the chemical composition ratio of NiO-GDC composites is successfully maintained during the sputtering process.

Fig. 3.7 FESEM-EDS data of the sputtered NiO-GDC film deposited on the AAO substrate (a) magnified FESEM image and (b)-(d) EDS composition maps of the film

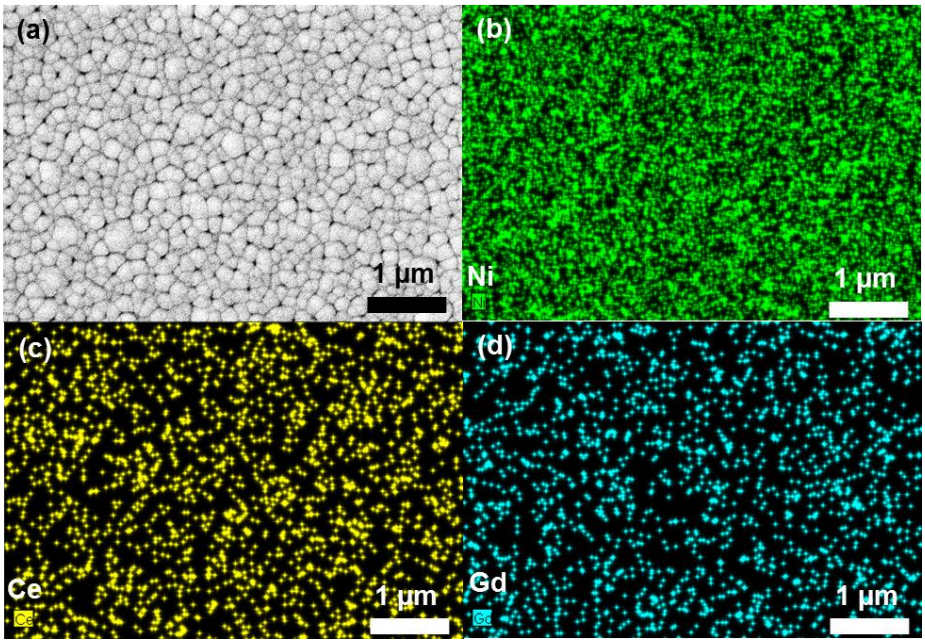

Cross-sectional images of the cells obtained using FIB-SEM are shown in figures 3.8 (a)-(c). In all figures, there are over four layers in the cells. Approximately 150 nm-thick porous Pt cathode is expected to provide an oxygen path for the oxygen reduction reaction (ORR) and maximize TPBs. Additionally, the approximately 600 nm-thick YSZ electrolyte layer has a fully dense structure. A few defects are discernible in figures 3.8 (b) and (c), but do not form a percolating path. From OCV values and I-V curves discussed in the following section, we confirmed that the isolated defects do not result in leakage current problem. The bottom-most AAO substrate seems to have several pores with 80-nm diameter, which are regarded as hydrogen gas channels. NiO-GDC or Ni/NiO-GDC bilayer anodes are shown between the AAO template and YSZ electrolyte. In addition, Ni/NiO-GDC interfaces were highlighted. A relatively bright layer above the AAO substrate was the Ni layer and the slightly dark thin layer above the Ni layer was the NiO-GDC MIECs layer. There is no noticeable difference in the surface morphology of the cathode and electrolyte between the TF-SOFCs. Surface images of Pt cathode and YSZ electrolyte are shown in figure 3.9. Therefore, the differences in electrochemical characteristics of the TF-SOFCs are assumed to originate from different anode structures.

Fig. 3.8 FIB cross-sectional images of sputtered NiO-GDC anode cells (a) without Ni layer (cell 4) and (b)-(c) with Ni layer (cell 5-6)

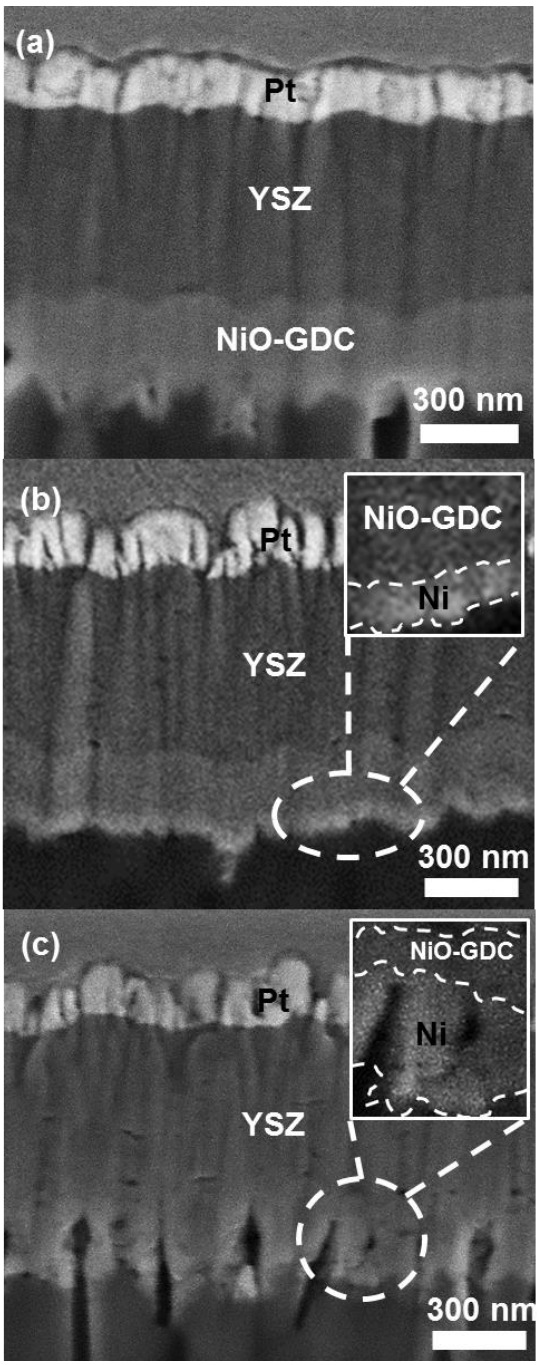

Fig. 3.9 FESEM-FIB surface images of cell 4, cell 5 and cell 6. (a)-(c) cathode and (d)-(f) electrolyte

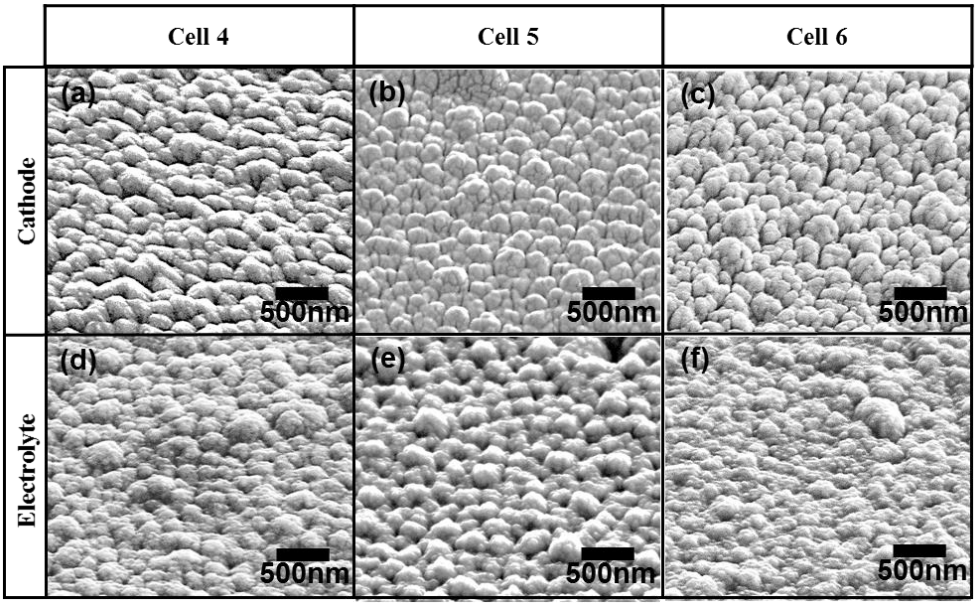

Polarization curves of the TF-SOFCs are presented in figure 3.10. First, the OCV values were 1.12, 1.13, and 1.13 V for cell 4, cell 5 and cell 6, respectively, at 500 ^{o}C. These were similar to previous values in μ-SOFC studies using nanoporous AAO substrate based YSZ electrolytes [3, 19-20, 24-26]. These results indicate that the pinhole free and gas-tight YSZ thin film electrolyte was successfully deposited on the nano-porous NiO-GDC or Ni/NiO-GDC anode. Additionally, similar OCVs of the TF-SOFCs mean that variations in Ni/NiO-GDC thickness ratios had negligible effects on OCVs.

The maximum power densities of cell 4, cell 5 and cell 6 were 80, 170, and 132 mW/cm^2, respectively. Compared to cell 4, cell 5 exhibits more than a two-fold increase in maximum power density (80 mW/cm^2→170 mW/cm^2) when the 70 nm-thick Ni layer was added and the NiO-GDC layer thickness was decreased from 280 nm to 210 nm. Cell 6, however, exhibited lower performance than cell 5 (170 mW/cm^2→132 mW/cm^2), although the Ni layer thickness increased.

Fig. 3.10 I-V curves of cell 4, cell 5 and cell 6 at 500ºC

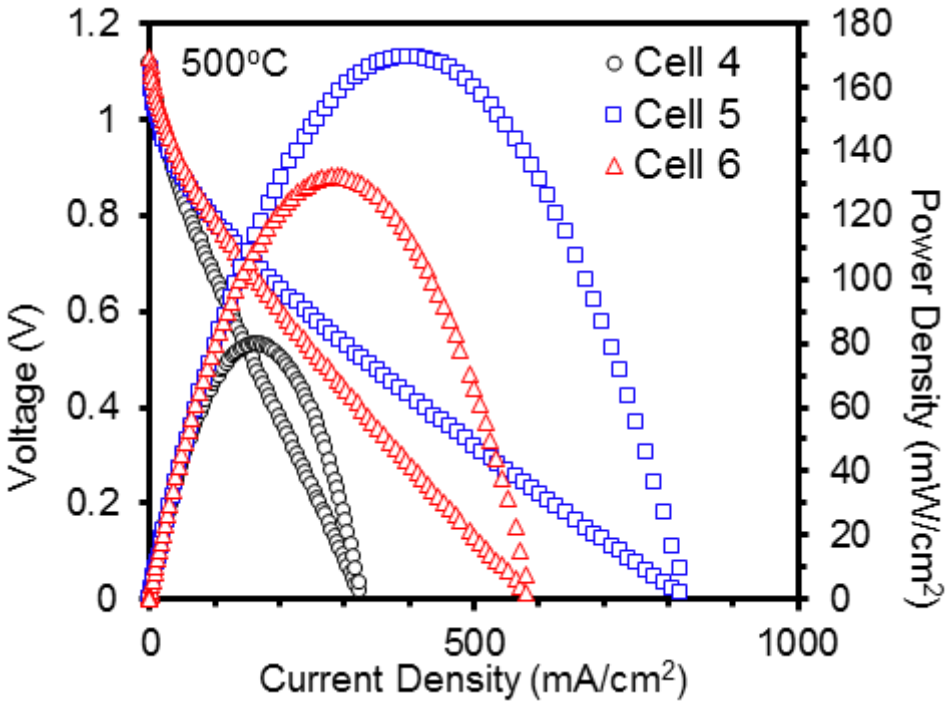

To investigate the resistances from the individual fuel cell processes, impedance spectra nyquist plots of the cells with different Ni/NiO-GDC thickness-ratios were obtained under 0.5 V bias at 500 ºC (Figure 3.11). The impedance spectra resistances were calculated by fitting to the equivalent circuit model and presented in table 3.1 [3, 20]. In the equivalent circuit model, R1, R2, R3, and R4 represent the electronic resistance, ionic resistance, anode polarization resistance, and cathode polarization resistance, respectively, in order of associated frequency ranges (higher to lower). The sum of high frequency resistances (R1+R2) is independent of the bias voltage and thus can be interpreted as ohmic resistance, *i.e.* the sum of electronic (R1) and ionic (R2) resistances. Impedance spectra nyquist plots of the TF-SOFCs at OCV and 0.5 V bias are shown in figure 3.12 [5]. R1+R2 were measured 1.69 $\Omega \cdot cm^2$, 0.96 $\Omega \cdot cm^2$, and 1.26 $\Omega \cdot cm^2$ for cell 4, cell 5, and cell 6, respectively.

There was a clear distinction among ohmic resistances considering that the ionic resistances (R2) for the cells are identical. The clearly distinctive ohmic resistances seem to stem from the different electrical contact resistances (R1). The ohmic resistances significantly decreased when the Ni layer was added to the anode (cell 4 vs. cells 5/6). As previously mentioned, the Ag paste was connected to the bilayer anode and the current was collected from the anode. Schematic of the current collecting mechanism in the bilayer anode is shown in figure 3.13. We speculate that there were two electron pathways from the TPBs region to the Ag paste. At cell 4, electrons are only transferred through pathway 1 (laterally through NiO-GDC). At cell 5 and cell 6, the Ni layer contributes to electron transport at the anode by acting as a current collector so that the electronic resistance can be reduced.

Fig. 3.11 (a) Nyquist plot of a impedance spectra under OCV at 500°C (b) EIS fitting model

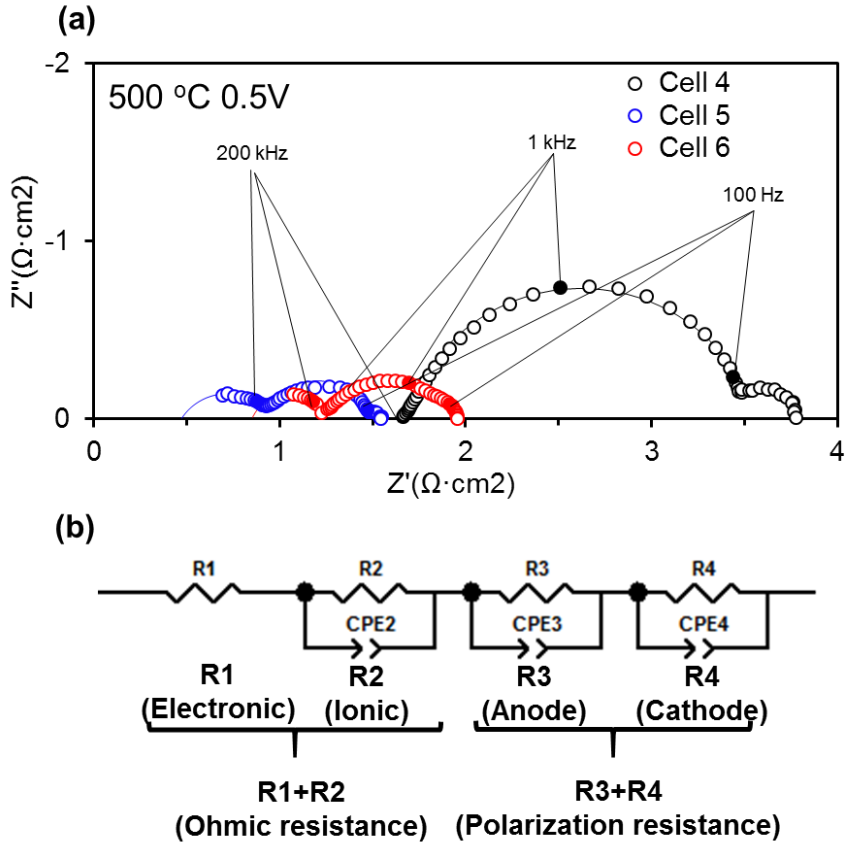

Fig. 3.12 Nyquist plot of the impedance spectra under OCV and 0.5 V bias at 500°C

(a) cell 4 (b) cell 5 (c) cell 6

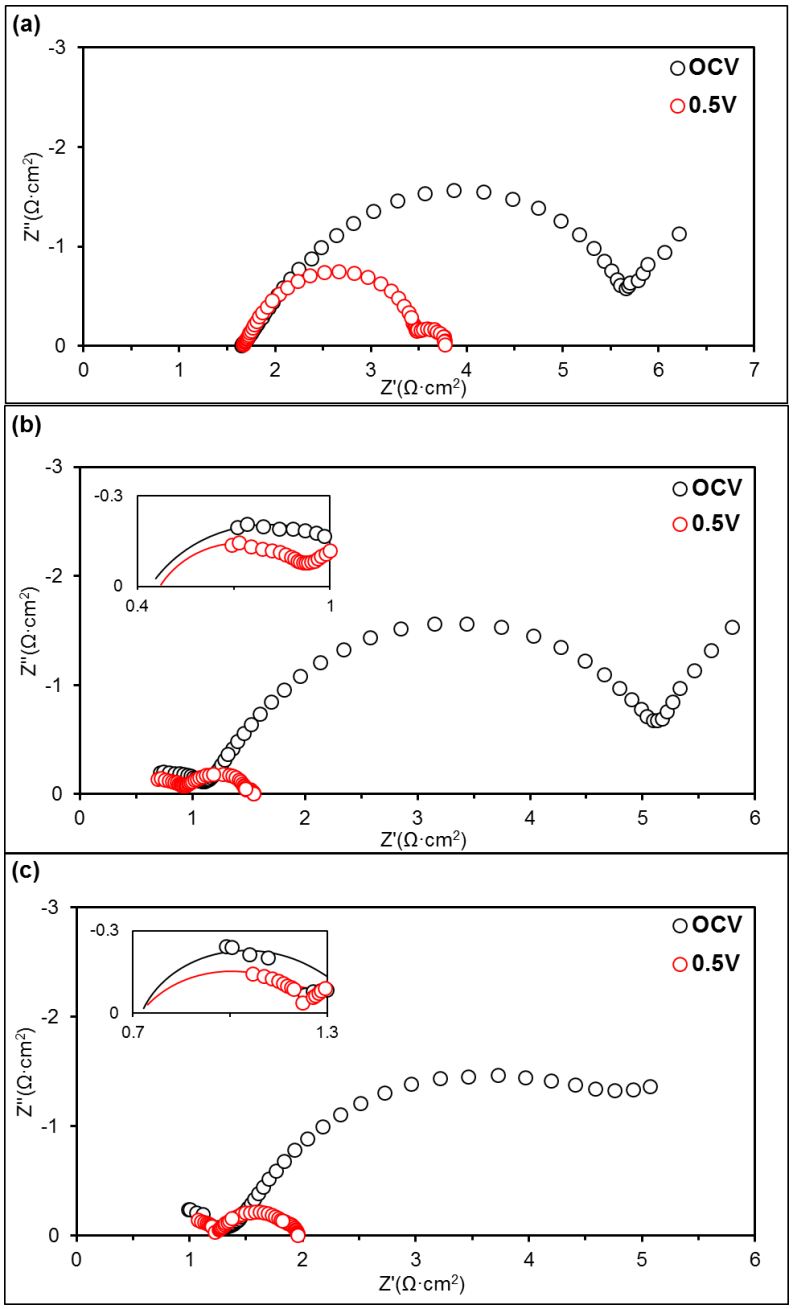

Fig. 3.13 Schematic of current collecting mechanism in the direct bilayer anode electron transfer to Ag paste (Pathway 1) via the Ni layer (Pathway 2)

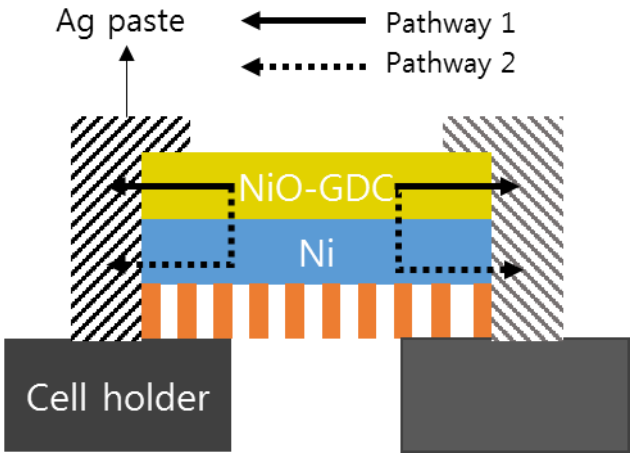

Table 3.1 Area-specific resistances of cell 4, cell 5 and cell 6 measured by EIS fitting model

	Cell 4	**Cell 5**	**Cell 6**
R1+R2 (ohmic)	1.69 Ω·cm²	0.96 Ω·cm²	1.26 Ω·cm²
R3 (Anode)	1.87 Ω·cm²	0.38 Ω·cm²	0.62 Ω·cm²
R4 (Cathode)	0.19 Ω·cm²	0.18 Ω·cm²	0.18 Ω·cm²

Semicircles associated with the anode and cathode polarizations are also observed in the 200 kHz - 100 Hz (intermediate frequency range) and < 100 Hz (low frequency range) frequency ranges, respectively [20, 27-28]. Considering all three cells have identical Pt cathodes, the difference in polarization resistance between cell 4 and cells 5-6 probably results from the anode side. Indeed, the cathode polarization resistances in all three cells at low frequency were identical at 0.18-0.19 $\Omega \cdot cm^2$. The anode polarization resistances of cell 4, cell 5, and cell 6 at intermediate frequency ranges were 1.87 $\Omega \cdot cm^2$, 0.38 $\Omega \cdot cm^2$, and 0.62 $\Omega \cdot cm^2$ under 0.5 V bias.

At the anode, the hydrogen oxidation reaction is known to occur in the following steps:[1] 1) hydrogen gas molecule (H_2) adsorption onto the catalyst surface, 2) dissociation of H_2 into hydrogen ions and electrons, and 3) incorporation of hydrogen ions into the bulk electrolyte at TPB. Among these steps, step 2 (dissociation of H_2) is usually rate-determining [1]. For cells 5-6, the hydrogen gas encounters the Ni layer before entering the porous NiO-GDC composites. In those cells, hydrogen molecules introduced into the anode may be more actively dissociated on the surface of the catalytic Ni surface than the case without the Ni layer. Hydrogen ions (protons) that are produced in such a manner may readily incorporate at the TPBs of the NiO-GDC composite. Although cells 5 and 6 may have lower TPB densities compared to cell 4 due to the thinner NiO, the anode polarization in those cells seem to largely benefit from fast hydrogen dissociation (Step 2), which results in smaller anode polarization resistances in cells 5 and 6 than in cell 4. In the meantime, a slight increase in anode polarization resistance in cell 6 compared to cell 5 (0.38 $\Omega \cdot cm^2 \rightarrow$0.62 $\Omega \cdot cm^2$) may

imply high TPB density loss due to the thin NiO-GDC layer (70 nm) adversely affecting the anode polarization. Therefore, fuel cell performance decreases despite better catalytic activities.

4. Conclusion

We analyzed the electrochemical performance of the TF-SOFCs comprised of (cathode) Pt | YSZ | NiO-GDC (anode) at the low temperature (500 ^{o}C). Anode thickness highly affected on the maximum power density, and the cell which had 320 nm-thick NiO-GDC anode showed the best performance (109 mW/cm^2). However, the ohmic resistance remained high (1.13 Ω·cm^2), and confined the cell performance. We tried to overcome the high ohmic resistance of the NiO-GDC anode cell by inserting nickel layer.

NiO-GDC thin film anode performance for the TF-SOFCs was enhanced by inserting an additional Ni layer between the NiO-GDC and the substrate. The TF-SOFC with 210 nm-thick NiO-GDC layer and 70 nm-thick Ni layer exhibited the best performance with 170 mW/cm^2, which was more than a twofold increase compared to that with 280 nm-thick NiO-GDC only anode (80 mW/cm^2). The EIS analysis showed that such a performance increase was due to the reduced ohmic and anode polarization resistances, which benefitted from additional current collection and catalytic activity by the Ni layer, respectively. The fuel cell performance decreased when the NiO-GDC layer became too thin compared to the Ni layer due to TPB loss. These results provide the essential TF-SOFC design rules where a proper thickness combination of the NiO-GDC and Ni layers is essential for maximizing the TF-SOFCs performance when employing the bilayer anode.

Reference

(1) R. O'Hayre, S. W. Cha, W. Colella, and F. B. Prinz, *Fuel Cell Fundamentals*, 2nd ed, Wiley, New Yorks **(2009)**.

(2) Y. Yoo, *J. Power Sources*, 160, 202–206 **(2006)**.

(3) S. Ji, I. Chang, G. Y. Cho, Y. H. Lee, J. H. Shim, and S. W. Cha, *Int. J. Hydrogen Energy*, 39, 12402–12408 **(2014)**.

(4) J. Park, J. Y. Paek, I. Chang, S. Ji, S. W. Cha, and S. I. Oh, *CIRP Ann. - Manuf. Technol.*, 62, 563–566 **(2013)**.

(5) J. An, Y. B. Kim, J. Park, T. M. Gur, and F. B. Prinz, *Nano Lett.*, 13, 4551-4555 (**2013)**.

(6) C. C. Chao, C. M. Hsu, Y. Cui, and F. B. Prinz, *ACS Nano*, 5, 5692–5696 **(2011)**.

(7) K. Kerman, B. K. Lai, and S. Ramanathan, *J. Power Sources*, 202, 120–125 **(2012)**.

(8) D. Beckel, A. Bieberle-Hütter, A. Harvey, A. Infortuna, U. P. Muecke, M. Prestat, J. L. M. Rupp, and L. J. Gauckler, *J. Power Sources*, 173, 325–345 **(2007)**.

(9) L. R. Pederson, P. Singh, and X. D. Zhou, *Vacuum*, 80, 1066–1083 **(2006)**.

(10) W. Z. Zhu, and S. c. Deevi, *Mater. Sci. Eng. A*, 362, 228–239 **(2003)**.

(11) H. J. Hwang, J. W. Moon, S. Lee, and E. A. Lee, *J. Power Sources*, 145, 243–248 **(2005)**.

(12) K. R. Reddy, and K. Karan, *J. Electroceramics*, 15, 45–56 **(2005)**.

(13) V. A. C. Haanappel, A. Mai, and J. Mertens, *Solid State Ionics*, 177, 2033–2037 **(2006)**.

(14) J. B. Goodenough, and Y. H. Huang, *J. Power Sources*, 173, 1–10 **(2007)**.

(15) T. Ishihara, T. Shibayama, H. Nishiguchi, and Y. Takita, *Solid State Ionics*, 132, 209–216 **(2000)**.

(16) J. Ayawanna, D. Wattanasiriwech, S. Wattanasiriwech, and K. Sato, *Mater. Manuf. Processes*, 29, 767–770 **(2014)**.

(17) M. Kim, Y. C. Ha, T. N. Nguyen, H. Y. Choi, and D. Kim, *Nanotechnol*. 24, 505304 **(2013)**.

(18) S. Ji, I. Chang, I, Y. H. Lee, M. H. Lee, and S. W. Cha, *Thin Solid Films*, 539, 117–121 **(2013)**.

(19) S. Ji, I. Chang, Y. H. Lee, J. Park, J. Y. Paek, M. H. Lee, and S. W. Cha, *Nanoscale Res. Lett.*, 8, 48 **(2013)**.

(20) J. Park, I. Chang,J. Y. Paek, S. Ji, W. Lee, S. W. Cha, and J. M. Lee, *CIRP Ann. - Manuf. Technol*., 63, 513–516 **(2014)**.

(21) J. Park, Y. Lee, I. Chang, W. Lee, and S. W. Cha, *Thin Solid Films*, 584, 125-129 **(2014)**.

(22) M. Mukhopadhyay, J. Mukhopadhyay, A. D. Sharma, and R. N. Basu, *Int. J. Hydrogen Energy*, 37, 2524–2534 **(2012)**.

(23) C. Xia, and M. Liu, *Solid State Ionics*, 152-153, 423–430 **(2002)**.

(24) C. W. Kwon, J. W. Son, J. H. Lee, H. M. Kim, H. W. Lee, and K. B. Kim, *Adv. Funct. Mater*., 21, 1154–1159 **(2011)**.

(25) S. Ha, P. C. Su, and S. W. Cha, *J. Mater. Chem. A*, 1, 9645 **(2013)**.

(26) I. Chang, S. Woo, M. H. Lee, J. H. Shim, Y. Piao, and S. W. Cha, *Appl. Surf. Sci.*, 282, 463–466 **(2013)**.

(27) S. B. Adler, *Solid State Ionics*, 111, 125–134 **(1998)**.

(28) T. Yamaguchi, H. Sumi, K. Hamamoto, T. Suzuki, Y. Fujishiro, J. D. Carter, and S. A. Barnett, *Int. J. Hydrogen Energy*, *39*, 19731–19736 **(2014)**.

국문초록

박막 고체산화물 연료전지의 성능향상을 위한 이중층 연료극의 최적의 두께비에 대한 연구

노 승 탁

기계항공공학부

대학원

서울대학교

이온/전자 혼성 전도체는 삼상계면을 넓힐 수 있고, 백금 기반 촉매를 대체할 수 있다는 장점이 있기 때문에, 각광을 받고 있다. 이번 연구에서는 NiO-GDC (연료극), YSZ (전해질), Pt (공기극)으로 구성된 박막 연료전지의 전기화학적인 성능을 Potentiodynamic 기법으로 평가하였다. 셀의 모든 구성요소는 반응성 스퍼터링을 이용하였으며, 특히 이온/전자 혼성 전도체인 NiO-GDC 연료극의 두께가 셀의 성능에 미치는 영향을 알아보기 위하여, NiO-GDC 를 6 시간, 8 시간, 10 시간 동안 스퍼터링 증착한 3 개의 셀을 제작하였다.

전기화학적 성능평가는, 500도의 전기로에서 이뤄졌으며, 100 sccm의 수소기체를 연료극으로, 자연대류 상태의 공기를 공기극으로 공급하였다. 실험결과, 320 nm의 연료극 두께를 가지는 셀이 최고의 성능을 보였으며

(105 mW/cm^2), EIS분석결과, 연료극의 두께가 셀의 오믹 저항에 영향을 미친 것으로 나타났다. NiO-GDC와 같은 이온/전자 혼성 전도체 전극은 순수 금속 전극과 비교하여, 전기전도성이 떨어지는데, 이로 인해 전극에서의 오믹저항으로 인해 성능 감소가 발생할 수 있는 것이다.

따라서 상대적으로 높은 NiO-GDC 연료극의 오믹저항을 줄이기 위하여, 니켈을 연료극으로 추가하여, Ni/NiO-GDC로 이루어진 이중층 전극을 제작하였다. 니켈층을 NiO-GDC 층과 AAO 지지체 사이에 삽입하여, 전기화학적 성능을 크게 향상하였다. Ni와 NiO-GDC 층의 두께비를 조절하여, 두께비가 성능에 미치는 영향을 확인하였고, 210 nm 두께의 NiO-GDC 층과 70 nm 두께의 니켈 층으로 연료극을 구성한 셀이 가장 좋은 성능을 보였다 (170 mW/cm^2). 니켈 층이 없는 셀에 비하여 크게 성능이 향상되었으며, EIS 분석결과 2가지 요인이 성능향상에 영향을 미쳤음을 확인 하였다. 첫째, NiO-GDC 층의 낮은 전기 전도성을 니켈의 훌륭한 전기 전도성으로 상쇄시켰다. 둘째, 니켈 층에서 수소의 산화반응이 활발하게 발생하여, 연료극에서의 활성화 저항을 줄일 수 있었다. 한편, 210 nm 두께의 니켈 층과 70 nm 두께의 NiO-GDC 층으로 구성된 셀은 132 mW/cm^{2}의 다소 낮은 출력을 보였는데, 이는 극도로 얇은 NiO-GDC 층에서 삼상계면의 영역이 줄어든 탓으로 보인다. 따라서 셀의 성능을 최대로 향상시키기 위해서는, 적절한 두께비를 가진 Ni/NiO-GDC 이중층의 구성이 무엇보다

중요하다는 것을 확인하였다.

주요어 : 니켈, 산화니켈-가돌리니아가 도핑된 세리아, 박막 고체산화물 연료전지, 이중층 연료극, 스퍼터

학 번 : 2013-23066